Journal of Fluids and Structures (1999) **13**, 709–722
Article No.: jfls.1999.0227 available online at http://www.idealibrary.com on IDEAL

VORTICES INCIDENT UPON AN OSCILLATING CYLINDER: FLOW STRUCTURE AND LOADING

M. Gaydon and D. Rockwell

Department of Mechanical Engineering and Mechanics, 19 Memorial Drive West, Lehigh University, Bethlehem, PA 18015, U.S.A.

(Received 8 April 1998 and in revised form 15 April 1999)

Interaction of an incident vortex street with an oscillating cylinder is addressed using high-image-density particle image velocimetry and simultaneous force measurements. This approach reveals that the timing of the incident vortices relative to the cylinder motion controls the large-scale vortex formation in the near-wake, and thereby the phase shift between the loading on the cylinder and its motion. As a consequence, it is possible to change the sign of the fluid-dynamic work done by the fluid on the cylinder. The incident vortices dramatically shorten the formation length of vortices in the near-wake and yield values of lift coefficient up to a factor of five larger than that for an isolated cylinder subjected to controlled oscillations in the absence of incident vortices. These alterations of the wake structure and loading occur in conjunction with globally locked-on patterns of incident and shed vortices with respect to the cylinder oscillation. Different states of global lock-on are attainable for different values of timing of the incident vortices.

1. INTRODUCTION

Interaction of incident vortices with a body, or more specifically a cylinder, represents a generic type of flow–structure interaction that occurs in a variety of engineering configurations, including heat exchanger tubes, adjacent tall buildings, piles of offshore platforms and bundled transmission lines. Practical scenarios involving these configurations are described by Naudascher & Rockwell (1980). The underlying flow physics associated with these and related types of interactions are reviewed by Rockwell (1998).

Zdravkovich (1987) classified the possible flow regimes for arrangements of circular cylinders in cross-flow, including a tandem arrangement of two cylinders. Arie *et al.* (1983) determined the unsteady lift and drag in relation to the unsteady surface pressure on the cylinder. In the event that the cylinders are elastic or elastically mounted, then the possibility of oscillation of the cylinders introduces an additional dimension of complexity. Chen (1985) and Zdravkovich (1985) addressed the mechanisms of fluid-elastic instability for cylinders in a tandem arrangement. King & Johns (1976) demonstrated the occurrence of both cross-flow and in-line oscillations in relation to modification of the patterns of vortex shedding.

For an array of a large number of cylinders, the flow patterns and the associated unsteady loading are particularly complex. Critical reviews of our knowledge base are given in the works of Païdoussis (1982), Chen (1984, 1987), Païdoussis & Price (1988) and Weaver & Fitzpatrick (1988). Recent insight into the flow patterns was provided by Ziada & Oengören (1992, 1993), who characterized the possible modes of vorticity shedding, which are a strong function of tube spacing. Price & Serdula (1995) visualized the coupled vortex shedding that can occur in a finite system of five risers.

0889–9746/99/060709 + 14 $30.00

For the simplified case of a spanwise coherent pattern of vortices incident upon an oscillating body, it is expected that the interaction will be a strong function of the timing, or phase shift, of the incident vortex pattern relative to the body oscillation. Indeed, as demonstrated by Jefferies & Rockwell (1996) for the case of a vortex incident upon a sharp leading-edge subjected to controlled oscillations, it is possible to generate fundamentally different patterns of vortex distortion and shedding at the edge. Moreover, patterns of vortices in a jet flow, which are incident upon an oscillating edge, undergo analogous distortions (Staubli & Rockwell 1987). Such distortions can be related to the direction of energy transfer between the fluid and the oscillating edge. Further investigations of controlled interactions of vortices with edges and corners are described by Kaykayoğlu (1989) for open-loop and by Gharib (1987) and Ziada (1995) for closed-loop active control systems. For the case of two oscillating cylinders in a tandem arrangement, Mahir and Rockwell (1996) have demonstrated, using qualitative flow visualization and pointwise velocity measurements, that attainment of locked-on patterns of vortices is a strong function of the phase angle between the cylinders. The importance of this phase shift was established in the investigations of Gopalkrishnan *et al.* (1994) and Streitlien *et al.* (1996) for the case of vortices incident upon an oscillating hydrofoil subjected to controlled motion. They found that energy in an array of incident vortices can be exploited to enhance efficiency and defined the type of vortex-hydrofoil encounter that yielded the highest propulsive efficiency.

The foregoing investigations have clearly established the importance of timing of the incident vortex(ices) with respect to the motion of an oscillating body. The following issues remain unclarified from a quantitative standpoint: (i) the possibility of globally locked-on patterns of vortices incident upon and shed from the cylinder; (ii) the relative contributions to the unsteady loading of the cylinder from the distortion of the incident vortices along the forward face of the cylinder, and alteration of the pattern of vortices shed into the cylinder near-wake; (iii) the degree to which the timing of the vortices shed in the near-wake is controlled by the incident vortex–cylinder interaction; and (iv) the nature of the fluid dynamic work on the cylinder, for both fluctuating lift and drag components, in relation to the timing of the pattern of incident vortices. The present investigation aims to address these issues using a cinema technique of high-image-density particle image velocimetry and simultaneous acquisition of unsteady forces on the cylinder.

2. EXPERIMENTAL SYSTEM AND TECHNIQUES

Experiments were undertaken in a large-scale water channel specifically designed for optical diagnostics. The main test section has a width of 914 mm, a depth of 609 mm, and a length of 5000 mm. For the present experiments, the water depth was maintained at 540 mm. Flow conditioning is achieved by a 2 : 1 contraction upstream of the test section, with arrangements of honeycombs and screens to bring the turbulence intensity to a value less than 0·1%. The flow velocity was maintained at 27 mm/s. The Reynolds number based on the cylinder diameter was 700.

As shown in Figure 1, the experimental apparatus consisted of a 305 mm long cylinder having a diameter of 25·4 mm, mounted in a horizontal, cantilevered arrangement at a location midway between the free-surface and the bottom of the water channel. In order to minimize inertia effects, the cylinder was hollow, with a wall thickness of 1·6 mm, except for a window segment that was installed to preclude shadow effects when employing a technique of high-image-density particle image velocimetry. This window, which was 13 mm long and located at a distance of 102 mm from the end of the cylinder was filled with distilled water. Using this approach, it was possible to minimize refractive distortion of the laser sheet through the cylinder.

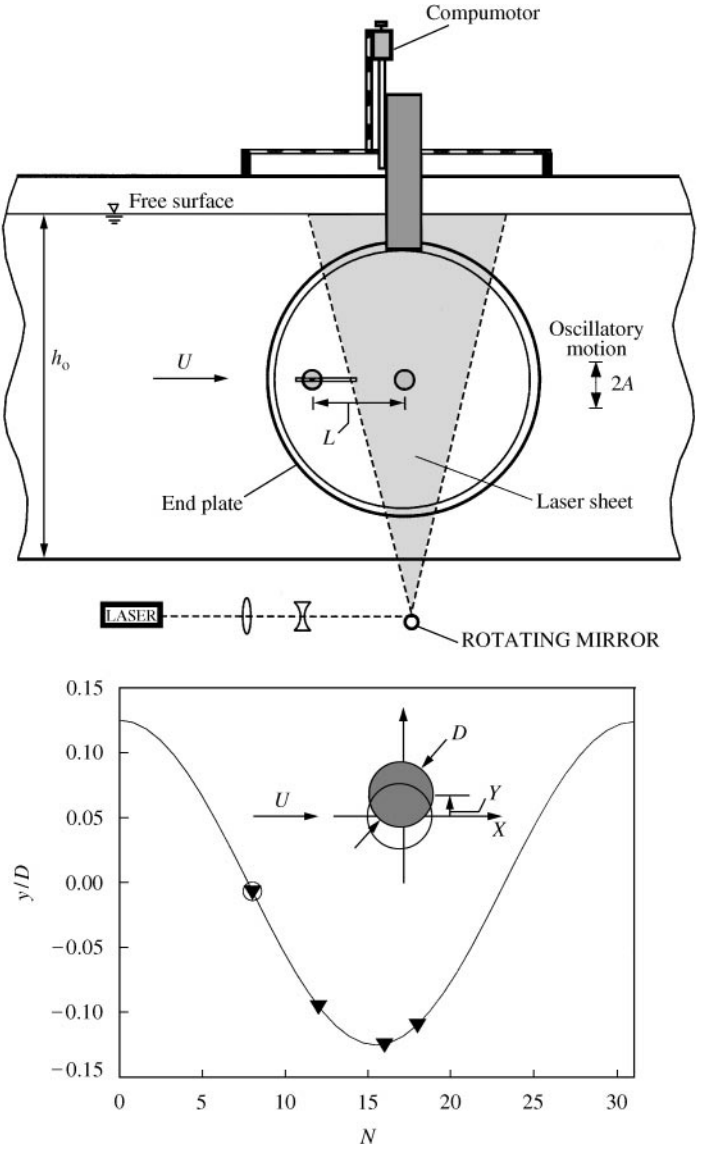

Figure 1. Schematics illustrating overview of experimental system, parameters for oscillating cylinder and one cycle of oscillation as a function of frame number N. Inverted triangular and circular symbols represent, respectively, images selected for cases with and without incident vortices.

The cylinder was mounted on a strain gauge sting in order to measure the unsteady lift and drag. The sting was 6·4 mm square brass stock. A total of eight strain gauges were located on the four faces of the sting. Before installation, an independent force calibration was performed on the strain gauge system by use of weights suspended at the end of the cylinder in air. The inertia force due to the finite mass of the oscillating cylinder was calculated from the dimensions and material properties of the cylinder, including the laser window. For the oscillation parameters of interest, the magnitude of the inertia force was subtracted from the measured values of force. As a further check on the correctness of interpretation on the forces measured from the cylinder-strain gauge system, the cylinder was subjected to controlled oscillations in quiescent water and the in-line force coefficients

were compared with those of Bearman *et al.* (1985). This check was performed for both axes of the strain gauge system for dimensionless amplitudes of the cylinder oscillation $2\pi A/D = 1$, 2 and 10. All values of lift coefficient C_L presented herein represent the total measured lift, which includes both the vorticity-based and so-called added-mass contributions to the lift force. The uncertainty of the lift and drag is estimated to be 2%.

The cylinder was mounted between circular end plates (368 mm diameter; 6 mm thick with 30° outward bevel). In order to generate a coherent pattern of vortices incident upon the cylinder, another cylinder of the same size was located a distance L upstream of the cylinder of interest. Slots in the end plates allowed the distance L to be varied from 110 to 163 mm. The entire apparatus, consisting of the cylinder and two end plates, was subjected to small-amplitude oscillations in the vertical direction. The amplitude of oscillation was $A/D = 0{\cdot}125$, which provided locked-on vortex shedding. In the case where two cylinders, i.e. an upstream and downstream cylinder, were mounted in the apparatus, both cylinders were subjected to the same oscillation amplitude; again, locked-on vortex formation occurred from the upstream cylinder, thereby providing a phase-repetitive system of vortices incident upon the downstream cylinder. Moreover, this scenario also promoted a global lock-on of the entire incident and shed vortex system from the downstream cylinder. As indicated in Figure 1, both cylinders were maintained at the same transverse location for all experiments. For both the single- and two-cylinder system, the oscillation frequency was 0·21 Hz, which corresponded to a Strouhal number of 0·21.

Preliminary experiments revealed that the timing of the concentrations of vorticity incident upon the downstream cylinder was important in determining the loading on the downstream cylinder. This timing is represented by the phase angle Φ_v. Angle $\Phi_v = 0^\circ$ is defined as the instant at which the centroid of the incident concentration of negative vorticity is located a distance of one cylinder diameter, D, upstream of the boundary of the cylinder, when the cylinder has its maximum velocity in the downward direction. Phase angle $\Phi_v = 180^\circ$ corresponds to an incident positive concentration of vorticity at the same location and at the same maximum downward velocity of the cylinder. These values of Φ_v were attained by adjustment of distance L between the cylinders; $\Phi_v = 0^\circ$ and 180° correspond to $L = 113$ and 155 mm.

A laser scanning version of high-image-density particle image velocimetry (PIV) was employed in a cinema mode, in order to acquire quantitative images simultaneously with the instantaneous lift and drag on the cylinder. This approach is described in detail by Rockwell *et al.* (1993). A continuous Argon-ion laser was employed with a maximum power output of 30 W. The scanning laser sheet was generated using one of two techniques. The first involved a galvanometer-driven oscillating mirror and the second employed a multi-(72)-faceted rotating polygon mirror. The flow was seeded with 12 μm silver-coated particles, and their multiply-exposed images were acquired using a motor-driven 35 mm camera, which allowed acquisition of 31 frames over one cycle of the cylinder oscillation. High-resolution (300 lines/mm) film was employed for recording the multiply-exposed particle images. A bias (rotating) mirror was located in front of the camera lens in order to preclude directional ambiguity of the particle image pattern. The pattern of particle images was evaluated using a single-frame, cross-correlation technique, with a window size of 80 pixels. A 50% overlap was employed during the interrogation process. The grid size in the plane of the laser sheet was 1·4 mm. A total of approximately 7000 velocity vectors were generated; images shown herein represent cropped versions of the overall velocity field. The uncertainty of the velocity is estimated to be of the order of 1%.

The image acquisition system for PIV and the oscillating cylinder system were controlled by a central laboratory microcomputer; this approach allowed synchronization of the image acquisition with the motion of the cylinder.

A schematic of the cylinder displacement y is given in the inset of Figure 1, which provides the time history of one cycle of the cylinder motion y/D as a function of frame number N of the recorded images. A sequence of 31 images was acquired over one cycle; only the most representative ones, designated by the triangular and circular symbols of Figure 1, are exhibited here.

3. NEAR-WAKE STRUCTURE IN ABSENCE OF INCIDENT VORTICES

Figure 2 shows patterns of vorticity, velocity and streamlines at an instant corresponding to the maximum (downward) vertical velocity of the cylinder. Patterns of velocity and streamlines in this figure, as well as in subsequent figures, are shown in a reference frame moving at $0{\cdot}70U$, where U is the freestream velocity. It was found, after comparing a number of reference frames, that $0{\cdot}7U$ provided the best comparison between streamline topology and patterns of vorticity. The layers of positive and negative vorticity extend a significant distance downstream of the base of the cylinder, thereby indicating a relatively long vortex formation length. This feature is characteristic of the near-wake structure in the so-called sensitive range of Reynolds number, as addressed recently by Lin *et al.* (1995), Chyu and Rockwell (1996), Prasad and Williamson (1997) and previous investigations cited therein. Visualization of the spanwise structure of the wake indicated that the process of large-scale vortex formation was phase-locked and thereby quasi-two-dimensional, i.e., locked-in along the span of the cylinder.

The velocity field and streamline pattern in a frame moving at 70% of the freestream velocity is shown in the right column of Figure 2. The image of the velocity field contains 4704 vectors. The originally acquired data included a total field of 7227 vectors; vorticity-free regions along the edge of the image were trimmed in order to conserve space. The streamline topology suggests elongated vortices corresponding to the layer of relatively distributed vorticity from the lower surface of the cylinder, and the layer originally formed

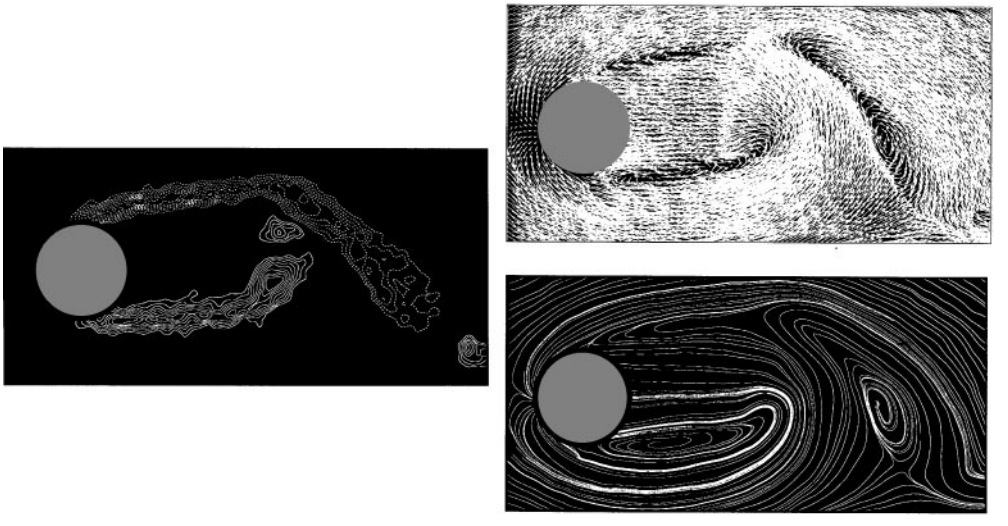

Figure 2. Representations of vortex formation from an oscillating cylinder in absence of incident vortices. Amplitude of cylinder oscillation is $A/D = 0{\cdot}125$ at a frequency $f_e = 0{\cdot}21$ Hz corresponding to the Kármán vortex formation from the stationary cylinder. Images illustrated correspond to the maximum vertical velocity of the cylinder ($N = 8$ in Figure 1). For contours of constant vorticity, $\omega_{min} = 2\,s^{-1}$ and $\Delta\omega = 1\,s^{-1}$. Velocity fields and streamline patterns are shown in a reference frame moving at $0{\cdot}70U$, where U is the freestream velocity.

from the upper surface of the cylinder, which extends across the wake. A well-defined saddle point exists at the lower right of the streamline pattern.

It is well established that this near-wake structure is sensitive to applied perturbations at the inherent Kelvin–Helmholtz frequency of the separating shear layers, originating with the study of Bloor and Gerrard (1966) and addressed by Chyu and Rockwell (1996), as well as in works cited therein. Moreover, alterations of the near-wake structure due to oscillations of the cylinder at or near the frequency of Kármán vortex formation are well known, as reviewed by Zdravkovich (1982), Williamson and Roshko (1988), Oengören and Rockwell (1988), Filler *et al.* (1991) and Nakano and Rockwell (1993, 1994). Relatively little is known, however, of the effect of incident, vorticity-bearing disturbances on the near-wake structure of an oscillating cylinder and the corresponding cylinder loading, as reviewed in detail in the Introduction. Most importantly, the possible mechanisms by which the near-wake is altered, or even controlled, by the timing of the incident vortical structures relative to the cylinder motion, remains unclarified. Central to our considerations is the distortion of the incident vortical structures along the forebody of the cylinder and the manner in which they evolve into the near-wake, while simultaneously inducing vortex shedding from the surface of the cylinder.

4. VORTICES INCIDENT UPON AN OSCILLATING CYLINDER: VORTEX DISTORTION AND SHEDDING IN THE NEAR-WAKE

The instantaneous vorticity field at crucial instants during the oscillation cycle of the cylinder is shown in the time sequence of images of Figure 3(a). The left column corresponds to a reference phase angle of the incident vortices of $\Phi_V = 0^\circ$ and the right column to $\Phi_V = 180^\circ$. The image numbers $N = 8$, 12, and so on, refer to the designation given in Figure 1. Images at a given value of N correspond to the same instantaneous position of the cylinder.

At $N = 8$, incident vortex E is negative (clockwise rotation) in the left column, whereas it is positive in the right column, meaning that the incident vortex street at this particular instant is 180° out-of-phase, i.e., shifted by one-half wavelength, when comparing images in the right versus the left column.

Furthermore, at $N = 8$, a large-scale negative vortex A appears in the near-wake at $\Phi_v = 0^\circ$ (left column); correspondingly, vortex A of positive vorticity contours appears at approximately the same streamwise position at $\Phi_v = 180^\circ$. In other words, the formation of vortices in the near-wake is approximately 180° out-of-phase. This is affirmed by comparing the patterns of vortices B and C at $\Phi_v = 0$ and 180° for $N = 8$; they are essentially mirror images of one another. A further distinction is that incident vortex D at $\Phi_v = 0^\circ$, which preceded vortex E, is split during its interaction with the cylinder; a portion travels above, and the remainder below the cylinder. On the other hand, the identity of vortex D is no longer discernible at $\Phi_v = 180^\circ$.

The tendency for vortices A, B and C to form approximately 180° out-of-phase in the left and right columns of images is further evident at $N = 12$, 16 and 18. Splitting of the incident vortex E is evident in both images at $N = 16$. A distinctive difference, however, is that at $\Phi_v = 0^\circ$, the incident vortex E is not split symmetrically, rather a major share of it progresses over the shoulder of the cylinder.

The corresponding patterns of instantaneous streamlines of Figure 3(b) show an approximate phase shift of 180° of the near-wake structure at the same value of N, e.g., the first and second rows of images representing $N = 8$ and 12. Therein, it is evident that the focus (center) of the large-scale vortex at $\Phi_v = 0^\circ$ is located at the upper right of each image, whereas it is located at the lower right of the image at $\Phi_v = 180^\circ$. Likewise, saddle points

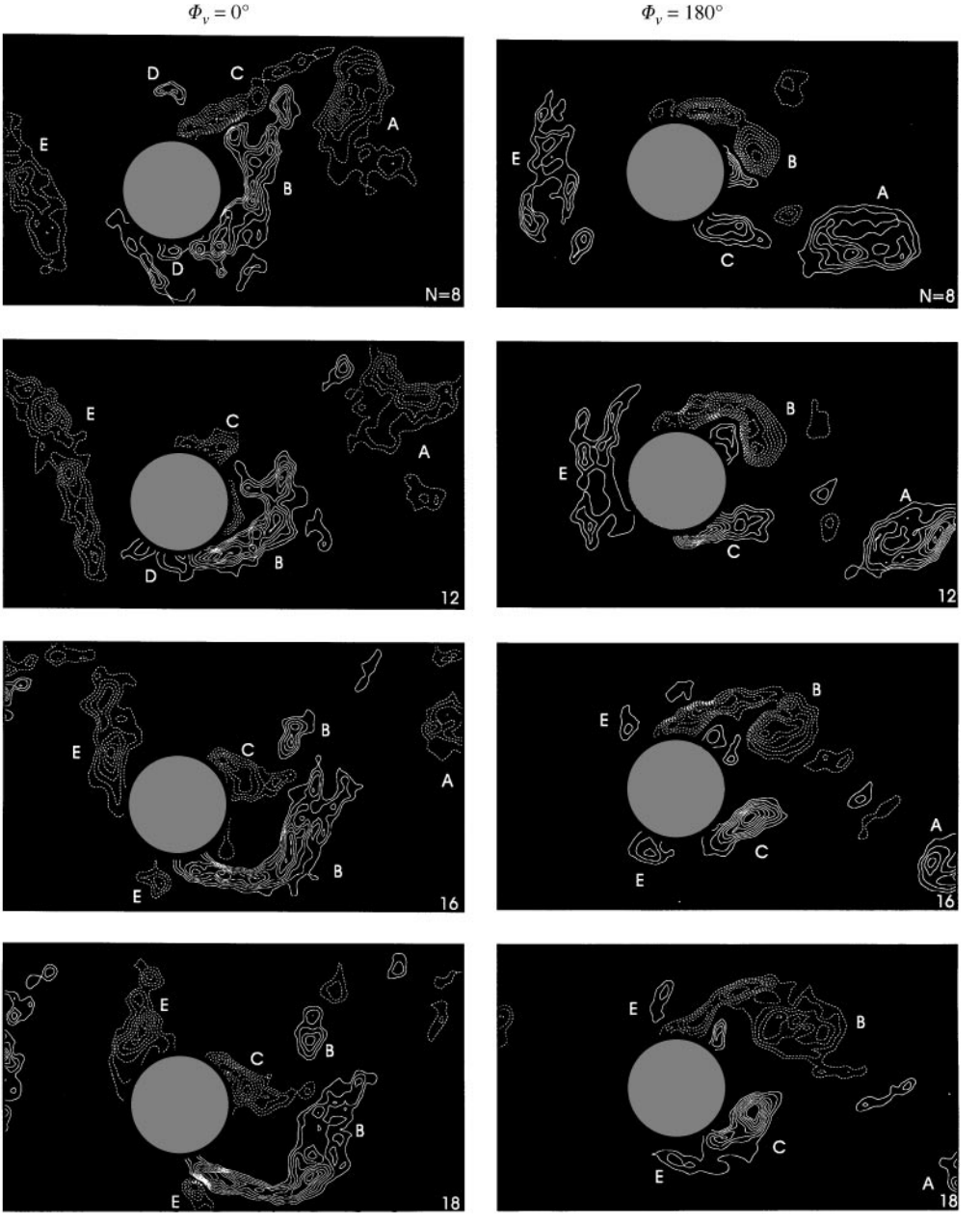

Figure 3(a). Images of contours of constant positive (solid line) and negative (dashed line) vorticity at selected instants during the oscillation cycle of the cylinder. Values of N are defined in Figure 1. Left column of images corresponds to a reference phase angle $\Phi_v = 0°$ of the incident vortex and right column represents $\Phi_v = 180°$. The cylinder undergoes oscillation at an amplitude $A/D = 0{\cdot}125$ and a frequency corresponding to the inherent Kármán frequency from the corresponding stationary cylinder. Minimum and incremental levels of vorticity are $\omega_{\min} = 2\,\mathrm{s}^{-1}$ and $\Delta\omega = 1\,\mathrm{s}^{-1}$.

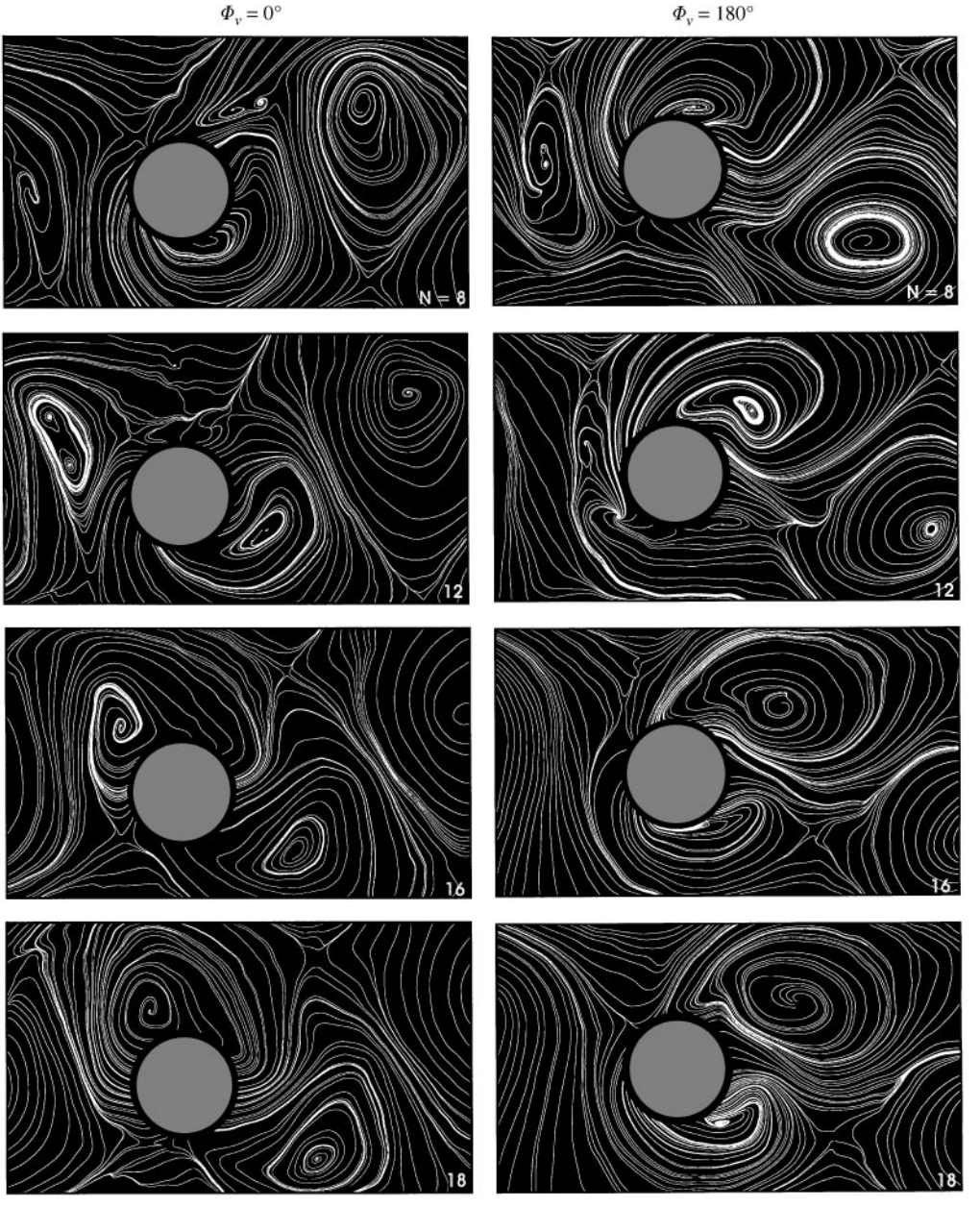

Figure 3(b). Instantaneous streamline patterns corresponding to the patterns of vorticity of Figure 3(a). All streamlines are shown in a reference frame moving at $0.70U$, in which U is the freestream velocity.

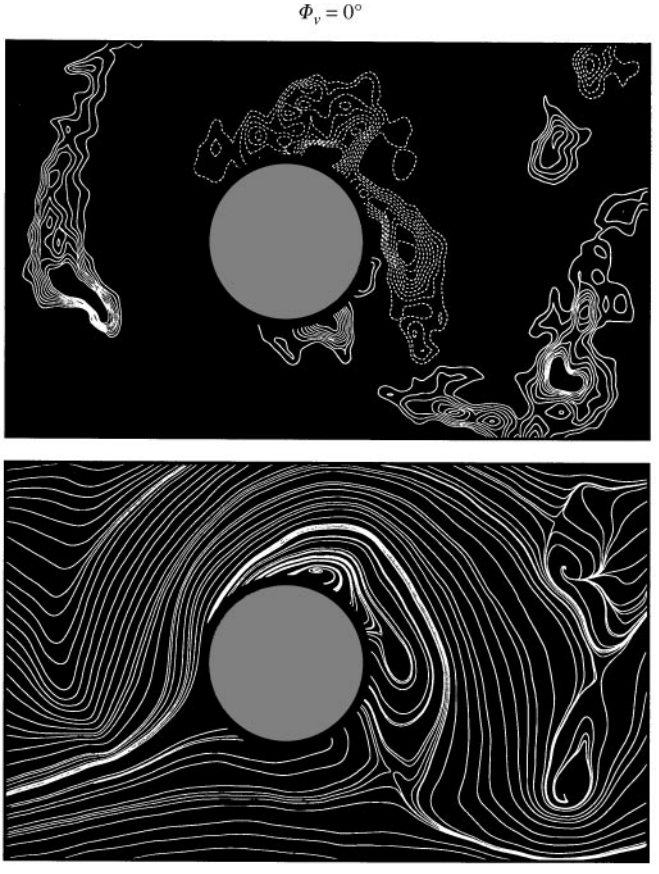

Figure 4. Illustration of the concept of vortex merging at separation. Negative (dashed line) vorticity contours along the upper shoulder and the base of the cylinder tend to form a single vortex. Minimum and incremental levels of vorticity are $\omega_{\min} = 2\,s^{-1}$ and $\Delta\omega = 1\,s^{-1}$. Corresponding streamline pattern is in a reference frame moving at $0{\cdot}70U$.

(intersecting streamlines) appear immediately beneath this spiraling pattern of vortex streamlines at $\Phi_v = 0°$, and above it at $\Phi_v = 180°$.

It is also evident in Figure 3(b) that the initially formed vortex from the lower surface of the cylinder at $\Phi_v = 0°$ is approximately 180° out-of-phase with that from the upper surface of the cylinder at $\Phi_v = 180°$. Furthermore, in the third row of images corresponding to $N = 16$, the large-scale vortex is formed from the bottom surface of the cylinder at $\Phi_v = 0°$, and a saddle point is located directly above it. This pattern is inverted at $\Phi_v = 180°$; the vortex spiral pattern appears at the top of the image with a saddle point immediately beneath it.

The distortion of the incident vortices E, already addressed in Figure 3(a), is represented in a different form by the streamline topology of Figure 3(b). At $\Phi_v = 0°$, in the images at $N = 16$ and 18, the focus of the large-scale spiral pattern moves up over the surface of the cylinder, whereas at $\Phi_v = 180°$, the identity of the split incident vortices is not detectable in the streamline patterns.

The possible interaction between patterns of incident and shed vorticity is a central feature of this class of vortex–body interaction. A later stage of development of the interaction at $N = 18$, $\Phi_v = 0°$ in Figure 3(a) is given in Figure 4. At this instant, corresponding to $N = 22$, it is evident that the split incident vortex E and the shed vortex C tend

to merge together before moving into the near-wake region. The corresponding instantaneous streamline pattern suggests a single, large-scale vortical structure.

Taking an overview of the sets of images corresponding to Figures 3 and 4 and comparing them with additional time sequences of incident vortices, it is evident that *global lock-on* of patterns of incident and shed vortices is attainable for extreme cases of phase shift of the incident vortices, i.e., $\Phi_v = 0^\circ$ and 180°. The forcing due to the incident vortex pattern appears to dominate, or at least attain compatibility with, the forcing due to motion of the cylinder. As a consequence, the entire pattern of incident, distorted and shed vortices in the left columns of Figures 3(a) and 3(b) is phase shifted relative to the corresponding pattern in the right columns at each respective value of N. The nature of splitting of the incident vortex, its interaction with the separating boundary layer along the cylinder and mutual induction effects between the incident and shed vortices apparently coexist in such a fashion that vortex formation from the surface of the cylinder occurs approximately 180° out-of-phase, even though the cylinder is in the same instantaneous position and has the same values of velocity and acceleration. It is expected that the aforementioned differences of the globally locked-on patterns of vortices are linked to a phase shift of the loading on the cylinder relative to its motion; the nature of this loading is addressed in the next section.

5. FORCES ON CYLINDER

Variations of the lift coefficient C_L with t/T are given in the top plot of Figure 5(a) for the cases of the stationary cylinder and the cylinder subjected to controlled oscillations in absence of incident vortices. The magnitude of C_L for the stationary cylinder is extremely

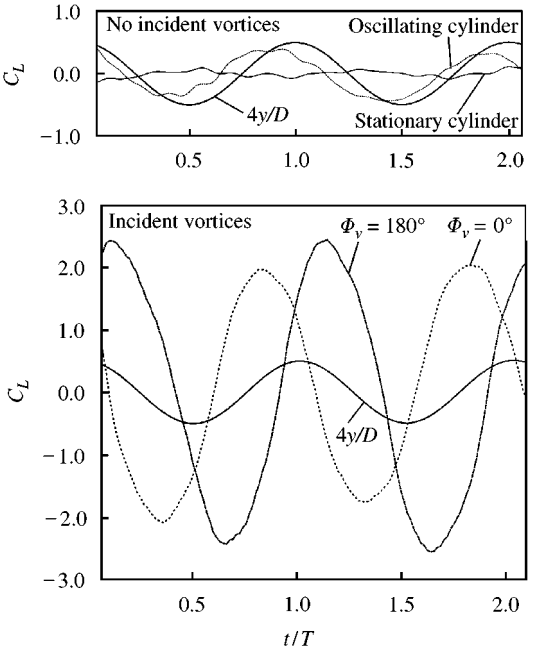

Figure 5(a). Variation of lift coefficient C_L as a function of time t/T, in which T is the period of the cylinder oscillation. The upper plot corresponds to the case of the cylinder in absence of incident vortices, while the bottom plot represents cases of incident vortices with phase angles $\Phi_v = 0$ and 180° with respect to the cylinder motion [compare Figures 3(a) and 3(b)]. As a reference, the instantaneous vertical position y/D of the cylinder is shown; it is multiplied by a factor of four, i.e., $4y/D$.

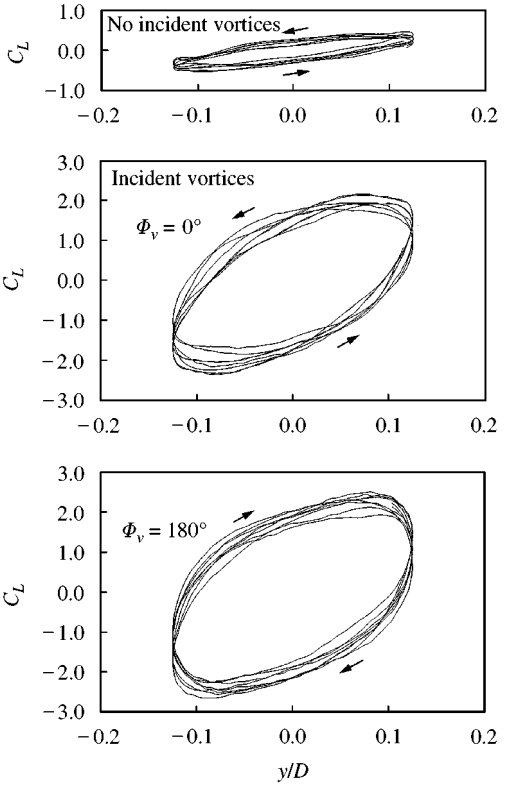

Figure 5(b). Trajectories of lift coefficient C_L versus vertical position of cylinder y/D for the cases of no incident vortices and incident vortices at $\Phi_v = 0°$ and 180°. Each representation corresponds to superposition of up to four randomly acquired samples C_L versus t/T.

small; it has an rms value of $(C_L)_{\text{rms}} \cong 0{\cdot}04$, which is in general agreement with the data of Szepessy and Bearman (1993). For the oscillating cylinder, the amplitude $(C_L)_0$ of the C_L trace is approximately $(C_L)_0 = 0{\cdot}4$, corresponding to a value of $(C_L)_{\text{rms}} = 0{\cdot}28$.

Variations of C_L for the case of the oscillating cylinder in presence of incident vortices are given in the bottom plot of Figure 5(a). It is evident that the value of the phase shift Φ_V of the incident vortices relative to the cylinder motion influences both the magnitude and phase of C_L. At $\Phi_v = 0$ and 180°, the magnitudes of the lift coefficient are $(C_L)_0 = 2{\cdot}0$ and 2·4 respectively, corresponding to rms values of $(C_L)_{\text{rms}} = 1{\cdot}4$ and 1·7. It is therefore evident that the vortices incident upon the cylinder at $\Phi_v = 0$ and 180° generate magnitudes of $(C_L)_0$ that are factors of 5·0 and 6·0 larger than $(C_L)_0$ for an oscillating cylinder in absence of incident vortices.

Regarding the phase shift of C_L, relative to the displacement of the cylinder y/D, the plot of Figure 5(a) shows that the peak of C_L at $\Phi_v = 0°$ lags the peak of y/D, while the converse is true for $\Phi_v = 180°$. This observation suggests that the work done by the fluid on the cylinder during the oscillation cycle will have different signs for $\Phi_v = 0°$ and 180°. Finally, it should be pointed out that the phase shift between the peak values of C_L at $\phi_v = 0°$ and 180° is not equal to π, rather it is approximately 0.6π. In order for the π relation to hold, it would be necessary for the incident vortices, their detailed distortion past the cylinder and the pattern of near-wake vortices at $\Phi_v = 0°$ to be exactly π out-of-phase with those at 180°; furthermore, the so-called added-mass contribution would have to be zero. As already

addressed in conjunction with Figures 3(a) and 3(b), the distortion of the incident vortex is distinctly different for $\Phi_v = 0$ and 180°, and the pattern of near-wake vortices, though generally exhibiting patterns of vortex formation that are π out-of-phase at $\Phi_v = 0$ and 180°, have significantly different values of circulation and overall structure.

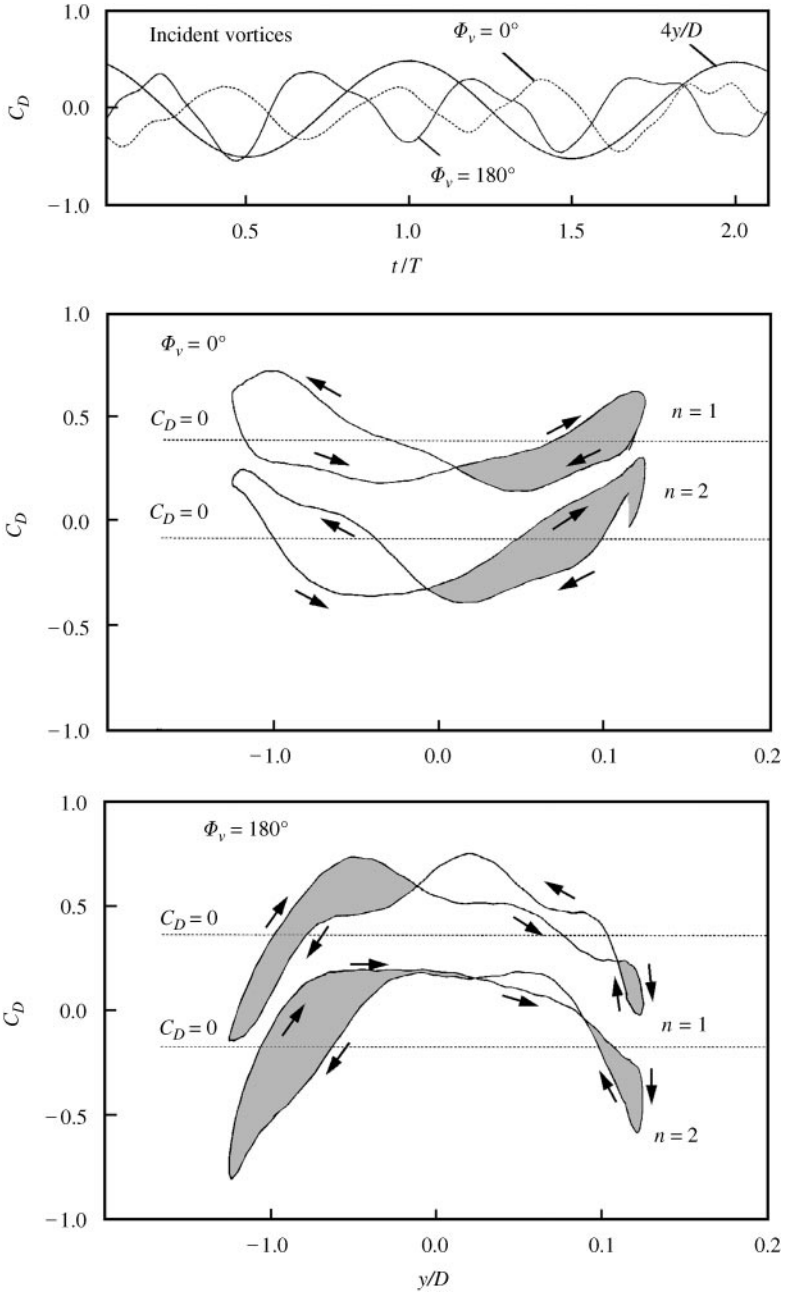

Figure 6: Variation of drag coefficient C_D with time t/T, in which T is the period of oscillation of the cylinder for cases of vortices incident upon the cylinder at values of phase angle $\Phi_v = 0°$ and 180°. Trajectories of C_D versus y/D are shown for two successive cycles of oscillation ($n = 1, 2$) at values of phase angle $\Phi_v = 0°$ and 180° of the incident vortices.

Plots of $C_L(t)$ versus $y(t)/D$ are given in Figure 5(b). They correspond to superposition of up to four randomly sampled time traces of $C_L(t)$, each having a duration of two cycles. For the case of no incident vortices, the trajectories of $C_L(t)$ versus $y(t)/D$ for successive cycles of oscillation are nearly coincident, in accord with the locked-on patterns of vortex formation of Figure 2. When vortices are incident upon the cylinder at $\Phi_v = 0^\circ$, as well as at 180°, the trajectories of C_L versus y/D for successive cycles are again relatively coincident, reaffirming the existence of globally locked-on patterns of incident, distorted and shed vortices. Particularly important for our considerations is the direction of the loops of C_L versus y/D. They are in the counterclockwise direction for (i) the case of no incident vortices, and (ii) for incident vortices with $\Phi_v = 0^\circ$. This observation indicates that the work done by the fluid on the oscillating cylinder is negative in both cases. In essence, this negative work corresponds to transfer of energy from the oscillating cylinder to the surrounding fluid. On the other hand, at $\Phi_v = 180^\circ$, the loop is in the clockwise direction, indicating that the work on the cylinder is positive, in turn signifying that the transfer of energy is from the fluid to the cylinder. In summary, the plots of Figure 5(b) show that a cylinder undergoing oscillations at a given amplitude and frequency can admit not simply one, but two globally locked-on states of unsteady loading, and the sign of the work can be opposite for these locked-on states.

Variations of the fluctuating drag coefficient C_D as a function of t/T are shown in the top plot of Figure 6 for the incident vortices at phase angles $\Phi_v = 0$ and 180°. Since these fluctuations of C_D occur at a frequency twice that of the cylinder motion, it is no longer appropriate to interpret a phase shift between the time variations of $C_D(t)$ and $y(t)/D$. It is appropriate, however, to compare the two cases of incident vortices at $\Phi_V = 0$ and 180°. The traces of C_D tend to be π out-of-phase, though significant distortion occurs over the total time of the trace.

Plots of C_D versus y/D are given at the bottom of Figure 6 for phase angles of the incident vortices $\Phi_V = 0$ and 180. Unlike the corresponding plots for C_L, these variations of C_D, which have a relatively low amplitude, exhibit significant distortion from one cycle to the next. Consequently, only two successive cycles, $n = 1$ and 2, are shown at each value of Φ_V. The reference axis $C_D = 0$ is shifted vertically, in order to allow identification of the phase diagram for each cycle. The general forms of the trajectories at $\Phi_V = 0$ and 180° tend to be inverted relative to each other; at $\Phi_v = 180^\circ$; however, the loops exhibit a significantly more complex pattern. The shaded regions correspond to the clockwise portion of the loops. Whereas the area of each positive loop is significant for $\Phi_v = 0^\circ$, it is nearly offset by the area of the corresponding negative loop. At $\Phi_v = 180^\circ$, the net area over the entire cycle is clearly positive, but again, there is significant distortion of the C_D versus y/D loops from cycle to cycle of the cylinder.

6. CONCLUDING REMARKS

It is well-known that locked-on vortex formation can occur from an oscillating cylinder in the absence of incident vortices. The present study focuses on a more complex form of lock-on, namely *globally locked-on* patterns of vortices incident upon the cylinder, their distortion along the cylinder, and shedding of vortices into the near-wake. It is possible to attain distinctly different states of global lock-on for excitation conditions that provide classical lock-on of vortex formation in the absence of incident vortices. The occurrence of these different states depends upon the phase shift, i.e., time of arrival, of the vortices incident upon the cylinder. During these locked-on states, the timing of the vortices shed into the near-wake is controlled by the incident vortex–cylinder interaction. In contrast, for

the case of the cylinder in absence of incident vortices, the timing of the shed vortices is controlled by the vertical motion of the cylinder.

These different locked-on states generate, for the lift force, opposite signs of work done by the fluid on the cylinder over an oscillation cycle. This observation emphasizes the importance of specifying the timing of the incident vortex pattern upon the cylinder. For the case of the drag force, both positive and negative hysteresis loops can be generated over a given cycle of oscillation of the cylinder. In fact, for certain conditions, it appears possible to attain an approximate balance between the areas of positive and negative loops, such that the net area is extremely small.

All of these foregoing features are associated with dramatic changes in the patterns of vortex formation in the near-wake. First of all, the so-called vortex formation length is substantially shortened in presence of the incident vortices, i.e., vortices are formed very close to the base of the cylinder in the presence of incident vortices. This decrease of vortex formation length occurs for both of the extreme cases of timing of the incident vortices relative to the cylinder motion. This alteration of the wake vortex system, in conjunction with the incident vortices and their distortion along the cylinder, gives rise to relatively large magnitudes of the lift force; they exceed those corresponding to oscillation of the cylinder in absence of incident vortices by a factor of at least five.

The present study has focused on values of Reynolds number for which the formation length of vortices from the corresponding stationary cylinder is relatively long, and the magnitude of the base pressure is correspondingly small. Investigations are underway to determine the effect of the natural state of the wake from the stationary cylinder, such as that occurring at much higher or lower values of Reynolds number.

All of the characterizations of the patterns of vorticity, velocity fields and streamline topology addressed herein represent instantaneous slices of the flow. In view of the fact that the flow patterns exhibit a globally locked-on form, it is expected that the large-scale spanwise variations of the flow structure will be minimal. Small-scale structures are, however, expected to be present along the span of the wake and they may influence the detailed patterns of vorticity, velocity and streamlines. This aspect is currently under investigation using an orthogonal plane imaging technique, and will be reported in a future work.

ACKNOWLEDGMENTS

The authors are pleased to acknowledge the financial support of the Office of Naval Research under Grants #N00014-94-1-0815, P00001 and #N00014-94-1-1183, the National Science Foundation under Grant #CTS8922095, and the National Aeronautics and Space Administration under Grant #NAG-1-1885.

References

Arie, M., Kiya, M., Morya, M. & Mori, H. 1983 Pressure fluctuations on the surface of two circular cylinders in tandem arrangement. *ASME Journal of Fluids Engineering* **105,** 161–167.

Bearman, P. W., Downie, M. J., Graham, J. M. R. & Obasaju, E. D. 1985 Forces on cylinders in viscous oscillating flow at low Keulegan-Carpenter numbers. *Journal of Fluid Mechanics* **154,** 337-356.

Bloor, M. G. & Gerrard, J. H. 1966 Measurements on turbulent vortices in a cylinder wake. *Procedings of the Royal Society of London*, **A294,** 319–342.

Chen, S. S. 1984 Guidelines for instability flow velocity of tube arrays in crossflow. *Journal of Sound and Vibration* **93,** 439–455.

CHEN, S. S. 1987 *Flow Induced Vibration of Circular Cylindrical Structures*. Berlin: Springer-Verlag.

CHEN, Y. N. 1985 Flow-induced vibrations of in-line heat exchangers. In *Proceedings of ASME Symposium on Flow-Induced Vibrations*, Vol. 3 (eds M. P. Païdoussis, J. Chenoweth and J. M. Bernstein), pp. 163–170. New York: ASME.

CHYU, C.-K & ROCKWELL, D. 1996 Near-wake structure of an oscillating cylinder: Effect of control of shear-layer vortices. *Journal of Fluid Mechanics* **322,** 21–49.

FILLER, J. R, MARSTON, P. L. & MIH, W. C. 1991 Response of the shear layer separating from a circular cylinder to small-amplitude rotational oscillations. *Journal of Fluid Mechanics* **231,** 481–499.

GHARIB, M. 1987. Response of the cavity shear-layer oscillations to external forcing. *AIAA Journal* **25,** 43–47.

GOPALKRISHNAN R., TRIANTAFYLLOU, M. S., TRIANTAFYLLOU, G. S. & BARRETT, D. 1994 Active vorticity control in a shear flow using a flapping foil. *Journal of Fluid Mechanics* **274,** 1–21.

JEFFERIES, R. and ROCKWELL, D. 1996 Interactions of a vortex with an oscillating leading-edge. *AIAA Journal* **34,** 2448–2450.

KAYKAYOĞLU, C. R. 1989 Active control of a mixing layer by upstream influence from an oscillating edge. *Journal of Fluids and Structures* **3,** 1–16.

KING, R. & JOHNS, D. J. 1976 Wake interaction experiments with two flexible circular cylinders in flowing water. *Journal of Sound and Vibration* **45,** 259–283.

LIN, J.-C., TOWFIGHI, J. and ROCKWELL, D. 1995 Instantaneous structure of near-wake of a circular cylinder on the effect of Reynolds number. *Journal of Fluids and Structures* **9,** 409–418.

MAHIR, N. and ROCKWELL, D. 1996 Vortex formation from a forced system of two cylinders. Part I: Tandem arrangement. *Journal of Fluids and Structures* **10,** 473–490.

NAKANO, M. & ROCKWELL, D. 1993 The wake from a cylinder subjected to amplitude-modulated excitation. *Journal of Fluid Mechanics* **247,** 79–110.

NAKANO, M. & ROCKWELL, D. 1994 Flow structure in the frequency-modulated wake of a cylinder. *Journal of Fluid Mechanics* **266,** 93–119.

NAUDASCHER, E. and ROCKWELL, D. (editors) 1980 *Practical Experiences with Flow-induced Vibrations* (IAHR/IUTAM Symposium, Karlsruhe, Germany, 3–6 September 1979, University of Karlsruhe). Berlin: Springer-Verlag.

OENGÖREN, A. & ROCKWELL, D. 1988 Flow structure from an oscillating cylinder. Part I: Mechanisms of phase shift and recovery of the near-wake. *Journal of Fluid Mechanics* **191,** 197–223.

PAÏDOUSSIS, M. P. 1982 A review of flow-induced vibrations in reactors and reactor components. *Nuclear Engineering and Design* **74,** 31–60.

PAÏDOUSSIS, M. P. & PRICE, S. J. 1988 The mechanism underlying flow-induced instability of cylinder arrays in cross-flow. *Journal of Fluid Mechanics* **187,** 45–59.

PRASAD, A. & WILLIAMSON, C. H. K. 1997 The instability of the shear layer separating from a bluff body. *Journal of Fluid Mechanics* **333,** 375–402.

PRICE, S. J. & SEDULA, C. D. 1995 Flow visualization of vortex shedding around multi-tube marine risers in a steady current. In *Flow-Induced Vibration* (ed. P. W. Bearman), Proceedings of 6th International Conference on Flow-Induced Vibration, London, UK, 1–12 April; pp. 483–493. Rotterdam/Brookfield: A. A. Balkema Press.

ROCKWELL, D. 1998 Vortex-body interactions. *Annual Review of Fluid Mechanics* **30,** 199–229.

ROCKWELL, D., MAGNESS, C., TOWFIGHI, J., AKIN, O. & CORCORAN, T. 1993 High image-density particle image velocimetry using laser scanning techniques. *Experiments in Fluids* **14,** 181–192.

STAUBLI, T. and ROCKWELL, D. 1987 Interaction of an unstable planar jet with an oscillating leading-edge. *Journal of Fluid Mechanics* **176,** 135–167.

STREITLIEN, K., TRIANTAFYLLOU, G. S. & TRIANTAFYLLOU, M. S. 1996 Efficient foil propulsion through vortex control. *AIAA Journal* **34,** 2315–2319.

SZEPESSY, S. & BEARMAN, P. W. 1993 Analysis of a pressure averaging device for measuring aerodynamic forces on a circular cylinder. *Experiments in Fluids* **16,** 120–128.

WEAVER, D. S. & FITZPATRICK, J. A. 1988 A review of cross-flow induced vibration in heat exchanger tube arrays. *Journal of Fluids and Structures* **2,** 73–93.

WILLIAMSON, C. H. K. & ROSHKO, A. 1988 Vortex formation in the wake of an oscillating cylinder. *Journal of Fluids and Structures* **2,** 355–382.

ZDRAVKOVICH, M. M. 1982 Modification of vortex shedding in the synchronization range. *ASME Journal of Fluids Engineering* **104,** 513–517.

ZDRAVKOVICH, M. M. 1985 Flow induced oscillations of two interfering circular cylinders. *Journal of Sound and Vibration* **101,** 511–521.

ZDRAVKOVICH, M. M. 1987. The effects of interference between circular cylinders in cross flow. *Journal of Fluids and Structures* **1,** 239–261.
ZIADA, S. 1995 Feedback control of globally unstable flows: Impinging shear flows. *Journal of Fluids and Structures* **9,** 907–924.
ZIADA, S. and OENGÖREN, A. 1992 Vorticity shedding and acoustic resonance in an in-line tube bundle. Part I: vorticity shedding. *Journal of Fluids and Structures* **6,** 271–292.
ZIADA, S. & OENGÖREN, A. 1993 Vortex shedding in an in-line tube bundle with large spacings. *Journal of Fluids and Structures* **7,** 661–687.